

Evaluation of algorithms for fire detection and mapping across North America from satellite

Zhanqing Li,^{1,2} R. Fraser,³ J. Jin,¹ A. A. Abuelgasim,³ I. Csiszar,⁴ P. Gong,^{5,2} R. Pu,⁵ and W. Hao⁶

Received 10 October 2001; revised 15 February 2002; accepted 9 April 2002; published 31 January 2003.

[1] This paper presents an evaluation of advanced very high resolution radiometer (AVHRR)-based remote sensing algorithms for detecting active vegetation fires [*Li et al.*, 2000a] and mapping burned areas [*Fraser et al.*, 2000] throughout North America. The procedures were originally designed for application in Canada with AVHRR data aboard the NOAA 14 satellite. They were tested here with both NOAA 11 and NOAA 14 covering the period 1989–2000. It was found that the active fire detection algorithm performs well with low commission and omission error rates over forested regions in the absence of cloud cover. Moderate errors were found over semi-arid areas covered by thin clouds, as well as along rivers and around lakes observed from sun-glint angles. A modification to a fire algorithm threshold and the addition of a new test can significantly improve the detection accuracy. Burned areas mapped by satellite were compared against extensive fire polygon data acquired by U.S. forest agencies in five western states. The satellite-based mapping matches nearly 90% of total forested burned area, with the difference being mainly attributable to omission of some nonburned islands and patches within the fire polygons. In addition, it maps a significant area of burning outside the fire polygons that appear to be true fires. The 10% omission error was found to be caused mainly by three factors: lack or insufficient number of active fires, partial burning, and vegetation recovery after early season burning. In addition to total area, the location and shapes of burned scars are consistent with the ground-based maps. Overall, the two algorithms are competent for detecting and mapping forest fires in North America north of Mexico with minor modifications. **INDEX TERMS:** 3360 Meteorology and Atmospheric Dynamics: Remote sensing; 0315 Atmospheric Composition and Structure: Biosphere/atmosphere interactions; 1615 Global Change: Biogeochemical processes (4805); 3322 Meteorology and Atmospheric Dynamics: Land/atmosphere interactions; **KEYWORDS:** forest fire, biomass burning, remote sensing, carbon budget, climate change

Citation: Li, Z., R. Fraser, J. Jin, A. A. Abuelgasim, I. Csiszar, P. Gong, R. Pu, and W. Hao, Evaluation of algorithms for fire detection and mapping across North America from satellite, *J. Geophys. Res.*, 108(D2), 4076, doi:10.1029/2001JD001377, 2003.

1. Introduction

[2] Wildfire is a major natural disturbance that has tremendous impact on environment, humans and wildlife, ecosystem, weather, and climate. There appears to be an increasing trend of natural fire activity [*Weber and Stocks*, 1998] that coincides with the observed and predicted

climate-warming trend in mid- and high latitudes [*International Panel on Climate Change (IPCC)*, 1990; *Hansen et al.*, 1996]. In 2000, the United States encountered its worst fire season since 1910. Nearly 80,000 wildfires burned 6.8 (see NIFC.gov) million acres, with a corresponding fire fighting cost exceeding one billion dollars [*Ramsey and Arrowsmith*, 2001]. In Canada, the five most severe fire years recorded this century occurred after 1980, and the top three after 1989. It has been predicted that more frequent wildfires are likely to occur if current warming trends prevail. A warm climate not only facilitates drying of fuels, but also is accompanied by increased storm activity, which provides the lightning ignition source [*Williams*, 1992]. This is further compounded by the accumulation of fuel materials due to suppression practices, which may lead to more devastating fires. Global warming is caused by the buildup of greenhouse gases in the atmosphere [*IPCC*, 1995], while the latter is further affected by the former [*Crutzen et al.*, 1979; *Kaufman et al.*, 1990]. A major agent/process that dictates the feedback is fire that emits considerable amount of greenhouse gases into the atmosphere.

¹Earth System Science Interdisciplinary Center and Department of Meteorology, University of Maryland, College Park, Maryland, USA.

²Also at International Institute for Earth System Science, Nanjing University, Nanjing, People's Republic of China.

³Canada Centre for Remote Sensing, Ottawa, Canada.

⁴Office of Research and Applications, National Environmental Satellite Data and Information Service, National Oceanic and Atmospheric Administration, Camp Springs, Maryland, USA.

⁵Department of Environmental Sciences, University of California, Berkeley, Berkeley, California, USA.

⁶Fire Sciences Laboratory, Rocky Mountain Research Station, U.S. Department of Agriculture Forest Service, Missoula, Montana, USA.

[3] Although tropical fires are widespread and have been studied extensively [Hao *et al.*, 1996; Kaufman *et al.*, 1990, 1994; Levine *et al.*, 1995], forest fires in the temperate and boreal zone also have significant climatic impact due to much larger capacity of emissions of greenhouse gases and atmospheric aerosols. Boreal and temperate forests in North America account for more than 25 percent of the world's forests. They are subject to large and intense burning annually. Extensive periodic wildfires in the forest liberate huge amounts of carbon. At present, the poor knowledge on the amount of carbon released from forest fires is one of the major uncertainties in understanding and closing the global carbon budget and cycle [Tans *et al.*, 1990; Fung, 1996]. A considerable amount of global carbon uptake (~ 2 Gt/year) remains unaccounted for in the carbon budget. It was argued that the missing carbon might rest in the terrestrial biomes of the Northern Hemisphere [Tans *et al.*, 1990], in particular the temperate and boreal forests in North America, which could account for the bulk (1.7 Gt/year) of the missing carbon [Fan *et al.*, 1998]. Substantiation of this argument requires a much-improved estimate of carbon emission and sequestration associated with fire activity that was proved to be the primary factor driving carbon budget [Chen *et al.*, 2000].

[4] To this end, accurate and complete information on long-term fire activity at continental to global scales is required. Currently, fire information is, at best, "patchy" in terms of both spatial coverage and temporal continuity and the quality varies considerably. To remedy the problem, a major undertaking under the NASA's Land Cover and Land Use (LCLUC) program is underway to develop a fire inventory across North America from 1985 until the present using satellite data. Satellite remote sensing is the only feasible means of acquiring fire information on continental and global scales of relatively uniform quality. The advanced very high resolution radiometer (AVHRR) onboard the National Oceanic and Atmospheric Administration series of satellite has been demonstrated to be able to monitor both active fires and map burned fire scars [Dozier, 1981; Flannigan and Vonder Haar, 1985; Kaufman *et al.*, 1990; Pereira and Setzer, 1996; Li *et al.*, 2001]. Among the various sensors that have been employed for fire detection such as the GOES [Prins and Menzel, 1990], DMSP [Elvidge *et al.*, 1999], ATSR [Arino *et al.*, 2001], and MODIS [Kaufman *et al.*, 1998], AVHRR offers the longest global observation capability that can be used for both fire monitoring and mapping. As such, we are developing a long-term fire inventory by processing daily AVHRR 1-km data covering virtually the entire North American continent.

[5] This paper is mainly concerned with evaluation and modification of existing algorithms used for active fire detection and burned area mapping. Since they were originally developed for application across the Canadian boreal forest [Li *et al.*, 2000a; Fraser *et al.*, 2000], it is necessary to assess and improve, if warranted, their performance over a larger domain and longer duration. The study is focused on major fires occurred in 5 western states (Montana, Idaho, Nevada, Utah, and Wyoming) during the summer of 2000, although analyses are also presented on fire detection using satellite data covering a much longer period of time.

[6] The following section describes the data and algorithms used. Section 3 presents the results of fire detection across North America north of Mexico (hereafter referred to as NA) and modifications made to the algorithm. A detailed evaluation of burned area mapping for fires occurred in western United States is given in section 4. Section 5 is a summary of the study.

2. Data and Algorithms

2.1. Data

[7] AVHRR data acquired by a series of NOAA polar orbiting satellites from NOAA 9 through NOAA 14 are being employed to generate a long-term fire inventory in NA. Data used in this study are primarily from NOAA 14, but some images from NOAA 11 are also used for assessing the applicability of the algorithms that were derived for application to NOAA 14 data. So far, most fire studies have employed a small number of AVHRR scenes. Only a handful of efforts were made using a large volume of daily AVHRR images for fire detection such as the IGBP-DIS Fire initiative that produced a one-year global product of post fires [Justice *et al.*, 1996; Dwyer *et al.*, 1998], the World Fire Web network that monitors fires around the world on near real time basis [Grégoire *et al.*, 2001], and some regional fire monitoring programs [Setzer and Pereira, 1992; Li *et al.*, 2000a]. Most of the projects did not process any AVHRR data prior to 1990, although the data have been available for over two decades.

[8] There are two types of NOAA AVHRR data collected at a full resolution (nominally 1-km), namely, the Local Area Coverage (LAC), and High Resolution Picture Transmission (HRPT). LAC data are recorded onboard satellite and downloaded at two NOAA receiving stations and archived at the NOAA Satellite Active Archive (SAA). The SAA LAC data dated back to May 1985 [Gutman *et al.*, 2001]. Over North America, however, most of the 1-km data in the NOAA archive are from the HRPT receiving stations. There are many HRPT receiving stations operated in NA. HRPT data are supplemented by LAC data for regions outside the acquisition area of the HRPT stations. HRPT data have been compiled for a complete global coverage for several years starting in 1992 [Townshend, 1994].

[9] The bulk of data used here are HRPT data acquired at the satellite receiving station in Prince Albert, Saskatchewan, Canada. The data cover nearly the entire NA except for the southerly portion of Florida and part of Atlantic Canada. They were calibrated, geo-referenced, re-sampled and processed using an automated system called GEO-COMP-N [Cihlar *et al.*, 2002]. Calibration for visible (ch.1) and near-IR (ch.2) measurements employ time-dependent offset and gain values recommended by Rao and Chen [1996]. The thermal AVHRR channels (3–5) are calibrated using onboard blackbody reference. NA-wide composites are registered to Lambert Conformal Conic projection using an orbit model and high-resolution LANDSAT MSS and TM image chips, which typically yield a positional accuracy better than 1km in Canada.

[10] In the United States, the registration error is larger for some regions (mainly in the east) due to a lack or insufficient number of image chips acquired. Note that, as

the GEOCOMP-N system was setup for application in the United States, a total of 754 LANDSAT TM image chips acquired over the United States were implemented into the system. Most of the chips were acquired in different months of 1990, while some were acquired between 1985 and 1995. Their distribution is not uniform, denser in western (especially in California) than in eastern regions. In general, the accuracy of pixel location registered using these chips is better than one pixel but varies with the density of image chips. The original AVHRR data, having a variable pixel size, were re-sampled to a constant 1 km resolution. The algorithm of *Li et al.* [2000a] was coded in the system for near real-time operation at the Canada Centre for Remote Sensing during the fire season of 2000. At present, the system is being used to map fires occurring in NA by processing historical AVHRR data since 1985 at the University of California at Berkeley, with the majority of historical data from the NOAA archives and a small amount from the Canadian receiving stations operated by the Canada Centre for Remote Sensing (CCRS).

2.2. Algorithms

[11] In fire-related applications, AVHRR data have been most frequently employed to detect active fire hot spots [*Flannigan and Vonder Haar*, 1986; *Kaufman et al.*, 1990; *Setzer and Pereira*, 1991; *Justice et al.*, 1996; *Li et al.*, 1997, 2000a, 2000b; *Randriambelo et al.*, 1998]. In a recent review article, *Li et al.* [2001] discussed the physical principles, limitations, and recommendations for using AVHRR to detect fires. In essence, AVHRR channel 3 is highly sensitive to fires of a range of temperatures. It also registers high values for some bright and hot objects such as clouds, barren land, or sun-glint over water. As a result of thermal emission and solar reflection, AVHRR channel 3 can become saturated, rendering difficulties in discriminating fires from other hot or bright targets [*Kennedy et al.*, 1994; *Randriambelo et al.*, 1998]. Fire detection algorithms thus use additional information from other channels to minimize false hot spots. Almost all fire detection algorithms are empirical, as the thresholds used in various tests were determined through analysis of sample fires. As a result, a fire detection algorithm working well for one region/biome may not necessarily be valid to other regions/biomes. The problem can be alleviated, in principle, through the use of spatial contextual algorithms that contain variable thresholds instead of fixed ones [*Flasse and Ceccato*, 1996; *Harris*, 1996; *Justice et al.*, 1996]. However, the detection results obtained by these algorithms are often not optimized for regional applications [*Li et al.*, 2001]. Fire detection results from different algorithms can vary by several factors as they are applied to the same data sets [*Ichoku et al.*, 2002]. This underscores the importance of assessing fire detection algorithms and products to fully exploit the utility of AVHRR data [*Li et al.*, 2001]. Following a preliminary assessment, the algorithm developed at the CCRS [*Li et al.*, 2000a] was selected to detect active fires in NA, which has low commission and omission errors. The algorithm consists of a series threshold tests to mark potential fire pixels and to remove false fire alarms. As is shown in the following section, a couple of minor modifications are introduced to

improve detection accuracy in United States, primarily over nonforest regions.

[12] Since fire hot spots represent only “snapshots” of burning activity, the temporal composite of active fire distribution is typically smaller than the actual burned area. In addition to AVHRR thermal channels that are most useful for fire detection, shortwave channels convey a signal of vegetation change caused by fire. The change is often measured by the Normalized Difference Vegetation Index (NDVI) computed from radiance/reflectance in the visible (ch.1: 0.58–0.68 μm) and near infrared (ch.2: 0.73–1.1 μm) bands, although other indices have been proposed for mapping burned surfaces [*Pereira*, 1999]. After green vegetation is burned, NDVI decreases owing to a rise in Ch.1 reflectance and decrease in Ch.2 reflectance. Some fire mapping methods are based on differences between pre- and post-fire NDVI composites [*Kasischke and French*, 1995; *Martin and Chuvieco*, 1995; *Li et al.*, 2000b]. NDVI regression [*Fernandez et al.*, 1997] and examination of NDVI time trajectories [*Li et al.*, 1997] have also been found effective. A significant advantage of post-fire mapping is that, unlike hot spot detection, the indicator of fire remains detectable for a longer period over boreal and temperate forests, circumventing problems caused by cloud cover and limited diurnal sampling. NDVI differencing is therefore capable of mapping burned areas that could otherwise be missed by using active fire detection. A main drawback of NDVI differencing for burn assessment at regional or continental scales is that a large commission error may result from a NDVI decrease unrelated to fire [*Kasischke and French*, 1995; *Li et al.*, 2000b]. Decreases can be caused by other factors such as drought, seasonal vegetation senescence, timber harvesting, image misregistration, and cloud contamination in the post-fire composite. A further difficulty with the differencing method is that an effective threshold for separating burns will be spatially and temporally variable [*Kasischke and French*, 1995; *Fernandez et al.*, 1997]. To compensate for this variation, *Fernandez et al.* [1997] derived a dynamic threshold based on each pixel’s NDVI decrease relative to the NDVI difference variability within the a region surrounding each fire, while *Roy et al.* [1999] used results from an active fire detection algorithm to classify a burned area index change map.

[13] In light of these limitations, a hybrid method, named Hot spot and NDVI Differencing Synergy (HANDS) [*Fraser et al.*, 2000], is proposed for mapping burned areas in Canada. It was designed to cope with cloud cover and contamination problems encountered in detecting active fires and the noise problem inherent in NDVI composites. The algorithm consists of the following major steps. First, hot spots are confirmed as real fires by significant decreases in NDVI between pre- and post-fire NDVI composites. This process may exclude some real fires, but the key is to assure that all pixels selected are true fires. Second, NDVI statistics (mean and standard deviation) are computed from the confirmed active fire pixels that are used to identify burned pixels. This process may not identify all burned pixels, but the identified ones should be truly burned. Third, regional thresholds are determined from spatial contingency information and active fire flag that are used to reclaim missing burned pixels. Finally, pixels passed local thresholds were connected to create burned scar clusters. Any clusters that

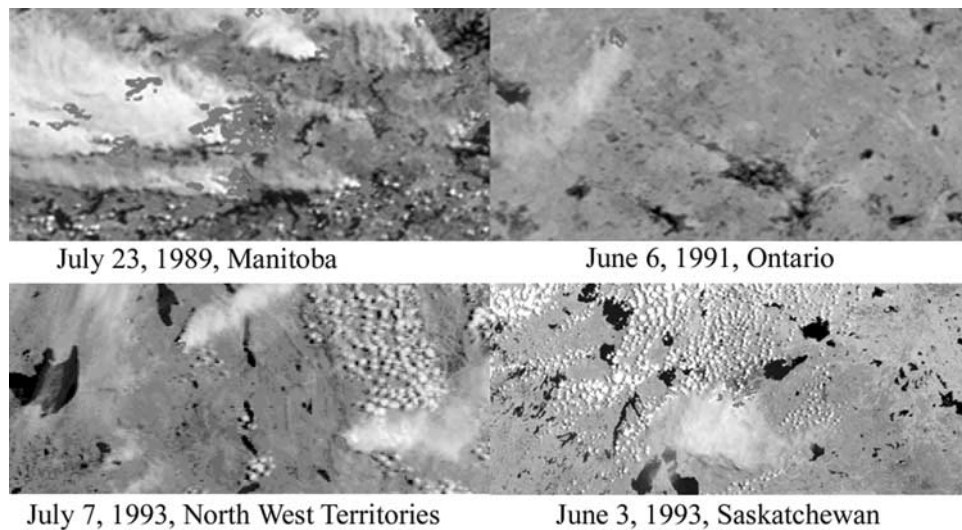


Figure 1. Fire locations identified using the algorithm of *Li et al.* [2000a] applied to different regions of Canada and different years spanning the lifetime of NOAA 11. Hot spots (red pixels) are superimposed over an AVHRR false color composite (RGB = 2, 2, 1). See color version of this figure at back of this issue.

contain less than 10% of confirmed hot spot pixels were eliminated, assuming that they are noise originated from the NDVI difference.

3. Application Results

3.1. Active Fire Detection

[14] Note that the fire detection algorithm of *Li et al.* [2000a] was designed for application with NOAA 14 data in Canada. Its application is now being extended across NA with AVHRR data acquired from other NOAA polar orbiting satellites, primarily NOAA 14, NOAA 11, and NOAA 9. Two tests were thus conducted: multi-year application to other satellites, and single-year application across entire NA.

[15] The first test was performed using sample scenes from AVHRR/NOAA 11 in 1989, 1991 and 1993. Note that the sensor functioned from 1989 to 1994. Subtle radiometric differences in the band-pass and spectral response function and the level of saturation in AVHRR channel 3 aboard different NOAA satellites have little impact on fire detection. However, changes in viewing geometry do impinge significantly on detection results. For example, near the end of the lifetime of AVHRR/NOAA 11 in 1994, satellite-viewing geometry is close to the principle plane. As a result of strong backscattering by vegetation, it is difficult to distinguish fires observed from backward directions. *Li et al.* [1997] developed an algorithm specifically for use with NOAA 11 1994 data that basically rejected all backward observations. Changes in background temperature are usually not significant enough to cause misidentification over boreal and temperate forests.

[16] To investigate whether the algorithm of *Li et al.* [2000a] is valid for application to NOAA 11 data, scenes containing fires that occurred in Canada were selected and the algorithms of *Li et al.* [2000a] and *Li et al.* [1997] were both applied. Figure 1 shows some detection results obtained over three different years (1989, 1991 and 1993)

in Manitoba, Saskatchewan, Northwest Territories, and Ontario. Three colors differentiate fires identified by both algorithms (red), by the NOAA 14 algorithm only (yellow), and by the NOAA 11 algorithm only (green). It is seen that both algorithms are able to identify the majority of fires very well. There is a general agreement between fires detected by the NOAA 14 algorithm and the NOAA 11 algorithm, as indicated by the overwhelming number of red spots. Fires identified by the NOAA 14 algorithm only are due to its more liberal detection criterion: $T3 > 315$ in comparison to $T3 > 316$ for the NOAA 11 algorithm. All these fires are confirmed by the ground-based fire reports from Canadian provincial fire agencies. Therefore, the algorithm of *Li et al.* [2000a] is suitable for processing both NOAA 14 and NOAA 11 data at least across Canada.

[17] To further test its applicability for use in NA, the algorithm was run daily across the United States and Canada throughout the 2000 fire season. Figure 2 shows the detection results for June 25 and July 23. Note that the active fire pixels are enlarged on the map for easy identification. While the algorithm detects most fires, some false fires were also produced, especially in southwest United States. The false fires occurred mostly at the edges of thin clouds over a range of warm and bright nonforest land cover types such as open shrub land, sparsely vegetated surfaces, pasture and range lands. The deterioration of performance under such conditions is understandable, given that the algorithm was originally developed to detect active forest fires over the Canadian boreal forest zone. Note, however, that the algorithm's performance over U.S. forest regions appears to be reliable. This is further demonstrated below.

[18] To better cope with the more diverse environment, the fire detection algorithm requires adjustments in the thresholds to accommodate other land cover types that are not common in Canada. Using a training database, two modifications were made for eliminating false fires. The first aims at eliminating false fires occurring at the edges of

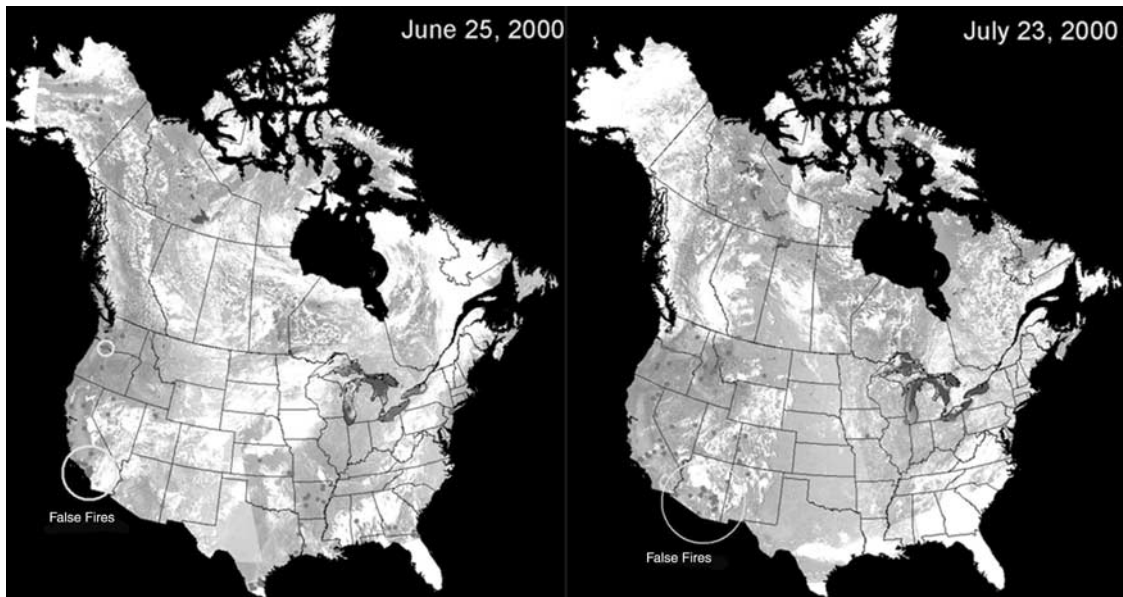


Figure 2. Active fire detection results across the United States and Canada for two sample dates during the summer of 2000 (hot spots are shown as enlarged red points, clouds appear white, vegetation is green, and yellow circles identify questionable results). See color version of this figure at back of this issue.

thin clouds over warm background. The second reduces false fires due to sun glint, visible along the Columbia River near the border between Washington and Oregon.

3.1.1. Modification 1

Old test $T4 - T5 \geq 4.1$ and $T3 - T4 < 19$

New test $T4 - T5 \geq 4.1$ and $T3 - T4 < 24$

[19] The basis of the modification lies in the fact that for thin cloud over a warm and bright surface, nonburned pixels can have rather high values in T3 relative to T4 due to increased solar reflection and thermal emission.

[20] There are two major constraints in selecting the threshold of T3-T4. One is that the new threshold should not undermine the detection over northern region dominated by forest ecosystem. Second, the threshold is confined to the saturation point of T3. Because of these constraints, AVHRR data suffer from an inherent problem that prevents fires from being detected over certain hot and sparsely vegetated land. For such scene types channel 3 is readily saturated during the summer due to excessive solar reflection and thermal emission. Yet, the brightness temperature in the thermal channel also becomes rather high. As a result, there is no distinct difference in T3-T4 between burned and

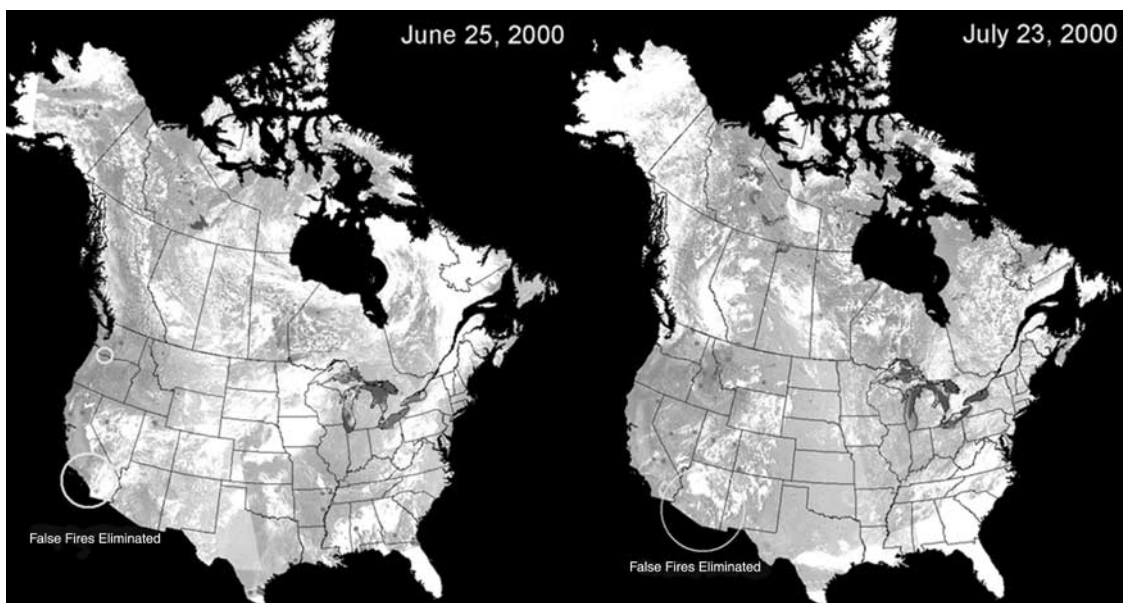


Figure 3. Same as in Figure 3, but based on the modified algorithm. See color version of this figure at back of this issue.

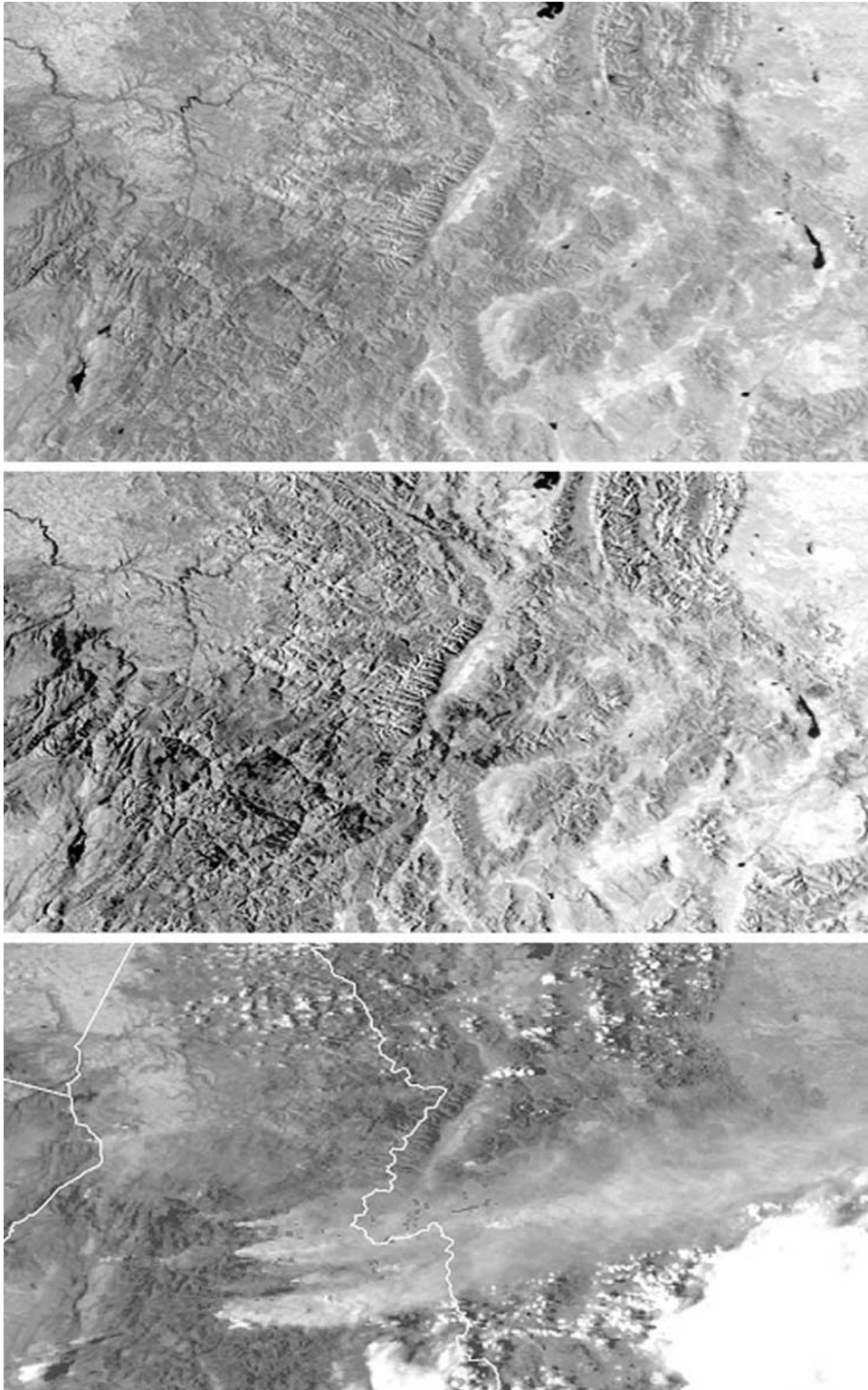


Figure 4. AVHRR clear-sky composites before (top) and after (middle) fires occurring in 2000. Bottom image shows fire hot spots detected on Aug. 26, 2000. See color version of this figure at back of this issue.

nonburned targets. By analyzing the inter-annual variability of T3 and T4, *Csiszar et al.* [2002] showed that fire detection is most feasible over forest, moderately difficult over other vegetation types (grassland, pasture, or cropland), and very difficult over sparsely vegetated bright surfaces such as open shrub and barren land.

3.1.2. Modification 2

[21] This modification is designed to eliminate falsely detected fires due to sun-glint. Sun-glint is mainly caused by water bodies and can be eliminated if we know exactly which pixels contain water. In practice, many sun-glint pixels contain only a small proportion of water and thus



Figure 5. The distributions of fire hot spots (a: left) and total burned area (b: right) detected from AVHRR across North America in 2000. See color version of this figure at back of this issue.

cannot be screened using a satellite-based land cover classification. This is due partly to registration error and partly to sub-pixel water. As a result, false fires are often observed along rivers and around lakes, as well as over unidentified small lakes (diameter less than 1 km). Owing to the large number of lakes and rivers in NA and especially Canada, observations are excluded if they were made within a 15° stereo angle surrounding the sun-glint direction (angle of specular reflection) and if the NIR channel is greater than 16%.

[22] The stereo angle (Θ) between a ray from the sun reflected specularly by the surface, and the viewing vector is given below:

$$\cos(\Theta) = \cos(\mu_1) \cos(\mu_2) - \sin(\mu_1) \sin(\mu_2) \sin(\varphi_1) \sin(\varphi_2) - \sin(\mu_1) \sin(\mu_2) \cos(\varphi_1) \cos(\varphi_2), \quad (1)$$

where

φ_1 = satellite azimuth angle;

μ_1 = satellite zenith angle;

φ_2 = solar azimuth angle;

μ_2 = solar zenith angle.

[23] Figure 3 shows similar results as in Figure 2 but using the revised algorithm. Many of the apparent false fires (e.g. those inside the circles and around big lakes) are eliminated. The majority of remaining active fires as detected correspond to the location of fires mapped by USDA Forest Service, although a handful of scattered false fires may still exist such as a couple of “fire” pixels detected around the Great Lakes region. More rigorous validation is given below in the context of mapping burned areas.

3.2. Burned Area Mapping

[24] The HANDS algorithm [Fraser *et al.*, 2000] used to map burned areas requires both a composite of active fire locations and pre- and post-fire NDVI composites. Two 10-day maximum NDVI composites for September 21–30 in

1999 and 2000 were produced by GEOCOMP-N. For regional and limited case studies, one may directly use single-date clear-sky images acquired before and after fire. Figure 4 presents clear-sky images in the western United States, where severe fires took place in the summer of 2000, together with an image showing fire hot spots detected on August 26, 2000. After burning, many fire scars are clearly visible, especially by comparing the two composites.

[25] Combining the NDVI and active fire composites, one can obtain a more accurate fire scar map. To do so, the following quantities were computed that are key variables of the HANDS algorithm: (1) The normalized NDVI difference was computed. To account for seasonal differences in growing condition between the two years, the NDVI composites are first normalized so that the mean NDVI values between the two years are the same. (2) Confirmed Burned Pixels (CBP) were computed. The hot spot pixels accompanied by a NDVI decrease are designated as “Confirmed Burned Pixels (CBP)”. The CBP are then used to calculate regional NDVI difference statistics. The CBP are also used to eliminate commission errors if within a burned cluster the number of CBP is less than 10% of total pixels. (3) The regional NDVI difference threshold was computed. Based on the mean and standard deviation of the NDVI difference for all CBP, regional NDVI difference thresholds were determined for each block of 200×200 km to isolate patches of potential burned pixels that were not identified as hot spots. (4) The local NDVI difference threshold was computed. This threshold retains pixels within each burned cluster with a NDVI decrease more than one standard deviation from the mean NDVI decrease of CBP. Comparison of the histogram of NDVI difference with the local NDVI difference threshold helps to explain the causes for commission or omission errors on the burned area mapping.

[26] Both the composites of hot spots and burned areas obtained from AVHRR using the two algorithms across NA’s forest areas in 2000 are presented in Figure 5. Detection results over nonforest regions are less reliable

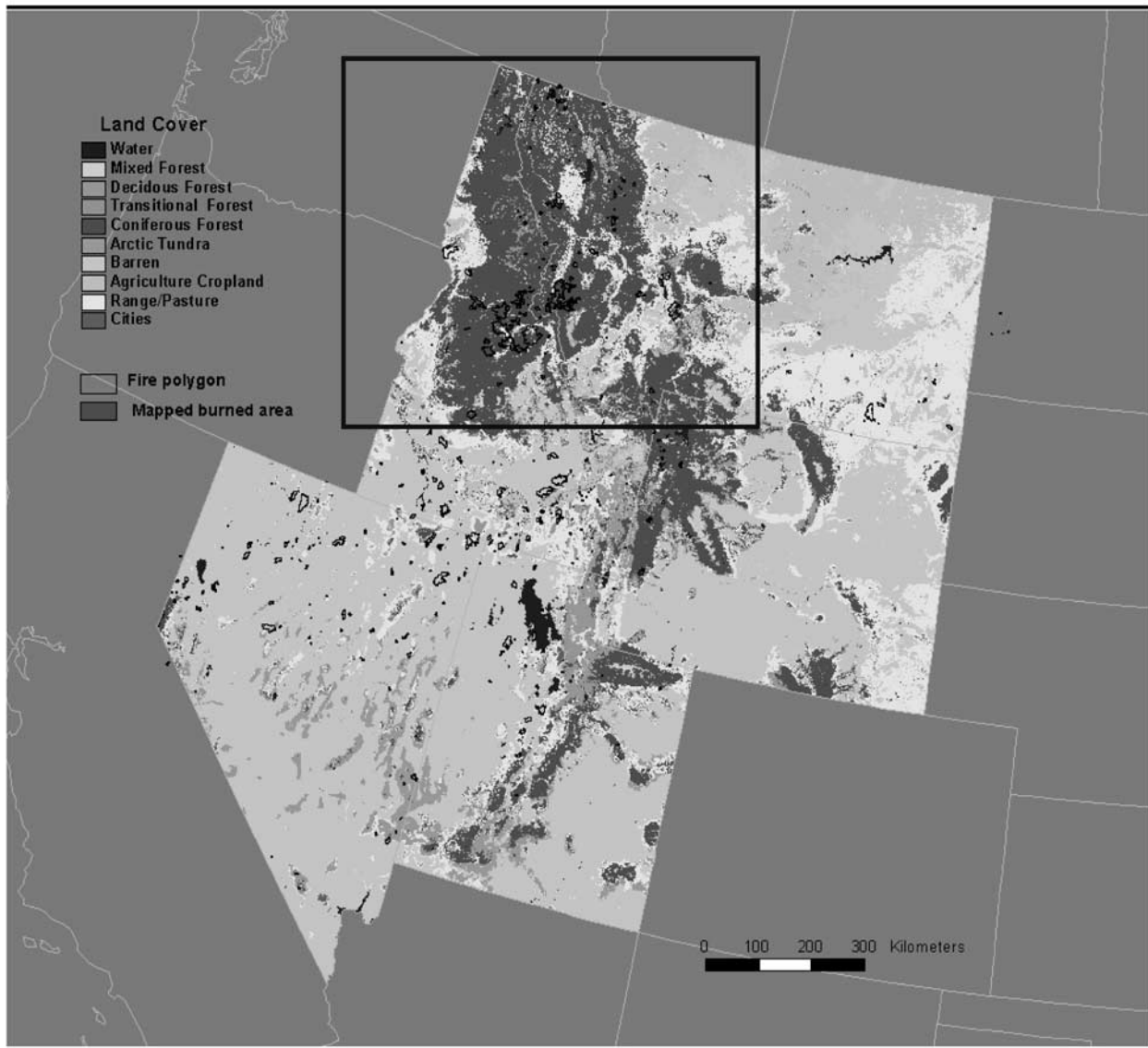


Figure 6. Comparison of satellite mapped burned area (red) and ground-based fire polygons in five western states. Background colors denote different land cover types. See color version of this figure at back of this issue.

and are addressed by *Csiszar et al.* [2002]. Major fires took place in Montana and Idaho. Many scattered fires were observed in both the United States and Canada with a rather low noise level. Due to the large spatial coverage and relatively small area of burning, the two maps look very similar. However, distinct differences do exist between the two when they are zoomed in small regions, as is shown in a more quantitative assessment presented in the following section.

4. Validation Analyses

[27] To quantitatively evaluate the performance of fire detection and mapping algorithms, wildfire burned area perimeters generated by the U.S. Forest Service are employed. Extensive ground-based fire perimeters are available as GIS polygons over five western states where wild-

fires were particularly active in 2000. Figure 6 shows a close-up comparison of fire polygons and burned areas mapped by the HANDS in this region. The base map shows land cover types aggregated from the IGBP-DIS AVHRR-based classification (<http://edcdaac.usgs.gov/glcc/glcc.html>). It is observed that the large fires occurring in coniferous forest regions are mapped accurately by the HANDS in terms of their size and shape. The majority of forest fire polygons are nearly entirely filled by burned area pixels from the satellite algorithm. By contrast, there are a numerous unidentified polygons over “barren” land. Note that the HANDS method is most effective for mapping burns in forested areas where active fire detection is reliable and burning produces a significant change in reflectance. A cursory browsing of AVHRR images indicates at least a portion of these polygons shows positive signs of burning (visible smoke plume) but usually last rather short periods.

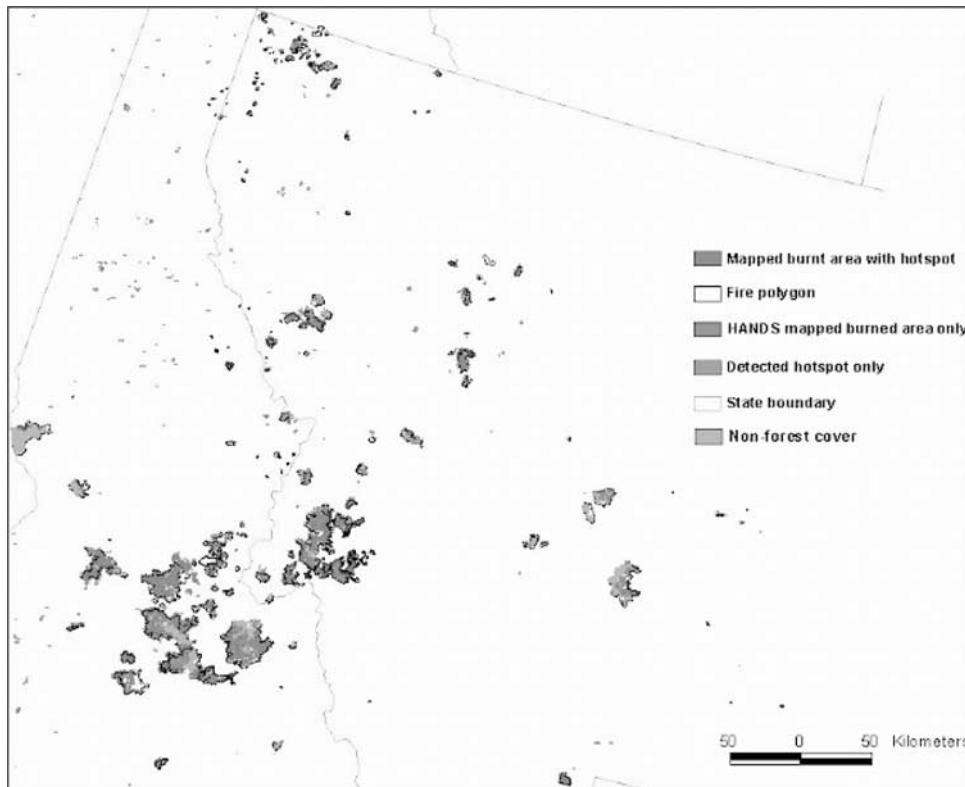


Figure 7. Fire mapping results classified by source and algorithm inside the selected area shown in Figure 7. Different colors differentiate between fire polygons, non-forest-covered regions, and state boundaries. See color version of this figure at back of this issue.

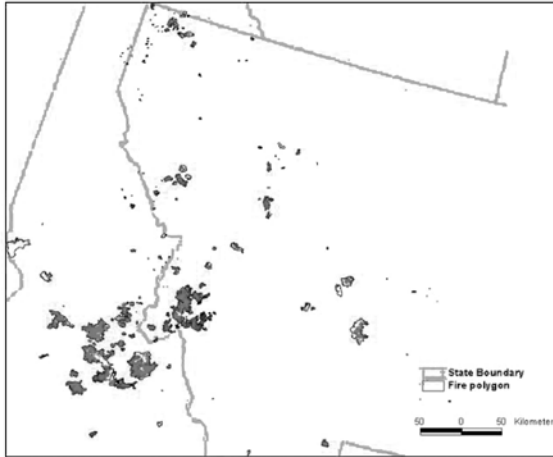
Although the land cover is unlikely to be truly barren land that has no vegetation to be burned, the biomass content of the vegetation is relatively low. As shown by *Csiszar et al.* [2002], fires occurred over such land cover type are most difficult, if not impossible, to detect. As the issue is addressed by *Csiszar et al.* [2002], the following analysis is limited to forest fires only.

[28] The HANDS mapped burned area covered 6369 pixels (km^2) for the five western states in forested area. 4327 pixels were inside wildfire polygons and 2042 pixels were outside the polygons. Inside the polygons, comparisons are made according to the following scenarios: (1) Pixels mapped by HANDS comprise 76% of total fire polygon area. This may be regarded as a conservative estimate of the accuracy of the satellite mapping method due to omission errors. Fires mapped by HANDS are supported by both hot spots and significant reduction in NDVI, which are thus most likely to be true burns. Actual mapping accuracy should be higher given scenario 2 and that fires missed by the polygon data may be picked by the satellite. (2) HANDS does not map 13% of the fire polygon area due to both lack of active fires and failure in passing the NDVI threshold tests. This potentially includes lightly or surface burned areas where the tree crown is largely intact, as well as unburned green islands. In generating the fire polygons by GPS from aircraft, nonburned islands within large burn scars are often not mapped. (3) Pixels not mapped by HANDS due to lack of active fires although NDVI thresholds are passed, which accounts for 8%. They are likely to be true fires but missed by HANDS, since the

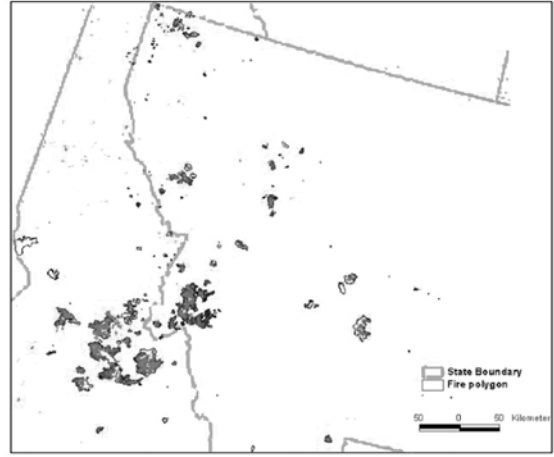
algorithm requires that potential burned areas contain a minimum 10 percent of CBP in order to minimize commission errors. In some cases, few or no active fires may be detected within a burn due to cloud cover, limited diurnal sampling, and failure of the fire detection algorithm. (4) Pixels not mapped on the perimeters of fire polygons, which accounts for 2%. They are “gray areas” as we are not sure if they are burned or not. It is more likely they are partially burned areas. (5) Pixels not mapped with active fires but failed in passing the NDVI tests which accounts for only 1%. This may result from early season burning in which the NDVI has recovered by the end of fire season. Misregistration is another likely cause. (6) A large number of pixels (2042) mapped by HANDS as burned area but missed by fire polygons. Most of those burned pixels were adjacent to fire polygons.

[29] To gain more insight into these statistics, Figure 7 shows a comparison of fire polygons and burned pixels identified with active fires (blue and green inside and outside the fire polygons, respectively) and without active fires (red). Nonforest areas are also marked inside the polygons. First, it is clear that overall satellite mapped burned areas match closely with the fire polygons. A significant proportion of the burned area mapped by HANDS does not have corresponding active fires. Area not detected within the fire polygons correspond to non-forest land cover. They are either unburned islands, or burning was so light that leaves little track seen by satellite. There are also scattered points or clusters identified as fires outside the fire polygons.

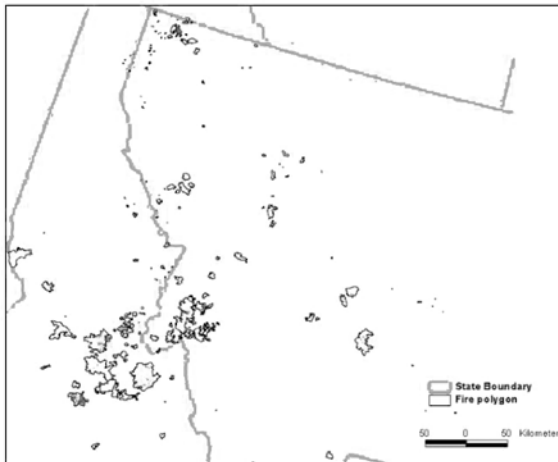
a all pixels inside the polygons



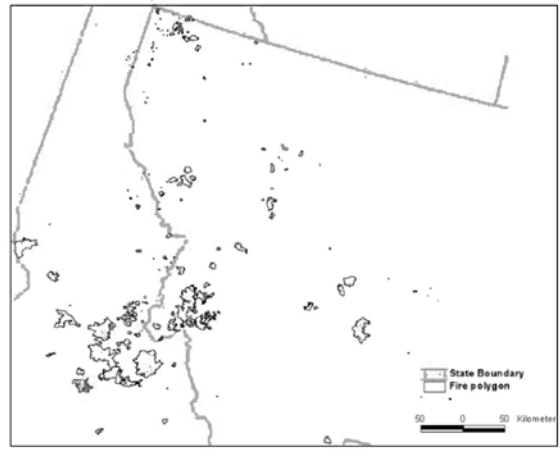
b all mapped fire pixels



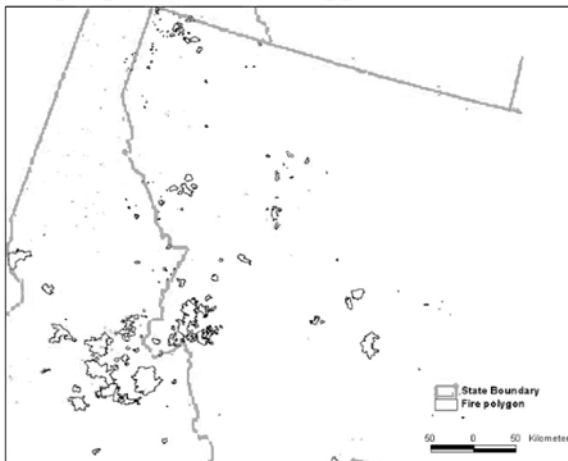
c pixels inside the polygons but not mapped



d fires not mapped for lacking hot spots



e hot spot pixels but not mapped



f mapped burned pixels outside the polygons

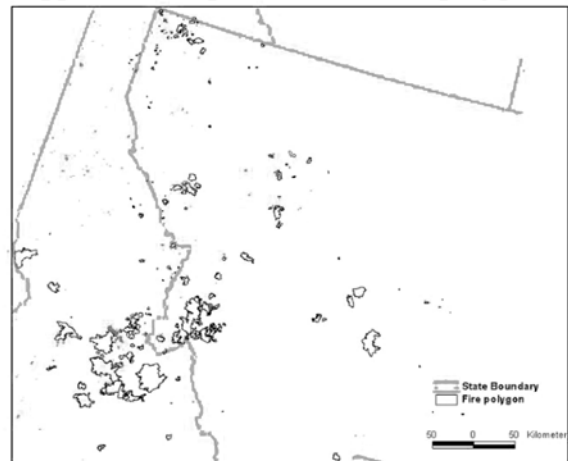
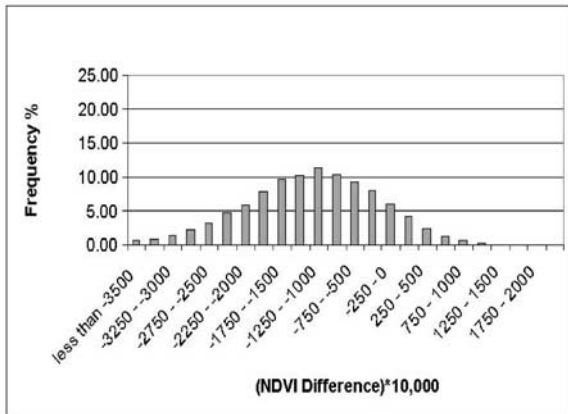


Figure 8. Analysis of fire detection results under different scenarios: (a) all pixels inside the fire polygons excluding nonforest regions, (b) all mapped fire pixels inside and outside the polygons, (c) pixels inside the polygons but not mapped, (d) inside the polygons not mapped due to lack of hot spots, (e) hot spot pixels but not mapped, and (f) mapped burned pixels outside the polygons. See color version of this figure at back of this issue.

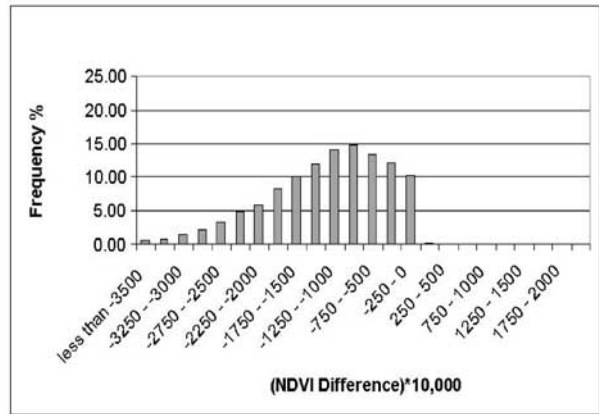
[30] To help understand the likelihood of burning, the spatial distribution of fire pixels (Figure 8) and the histograms of NDVI differences (Figure 9) are analyzed under different categories. Figures 8a and 9a show fire pixels

within the polygons (5593 pixels) regardless of satellite fire detection results. The histogram shows that 18.6% of pixels (1066) inside the polygons do not pass the regional NDVI difference threshold, which is why they are not mapped by

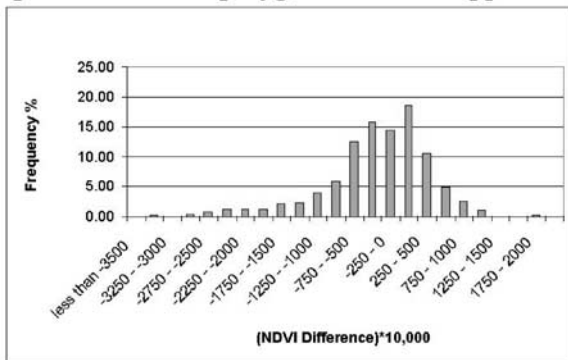
a. all pixels inside the polygons



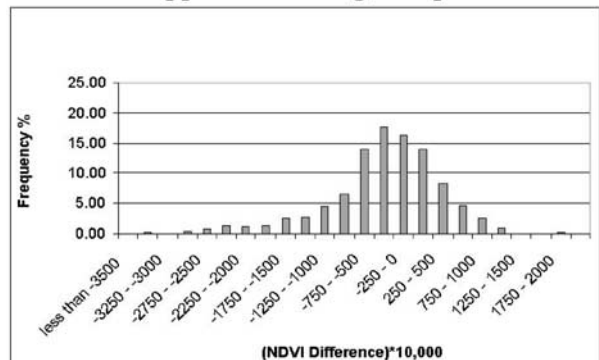
b. all mapped fire pixels inside the polygons



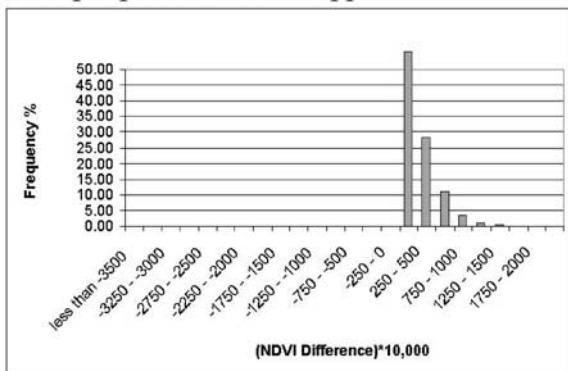
c. pixels inside the polygons but not mapped



d. fires not mapped for lacking hot spots



e. hot spot pixels but not mapped



f. mapped burned pixels outside the polygons

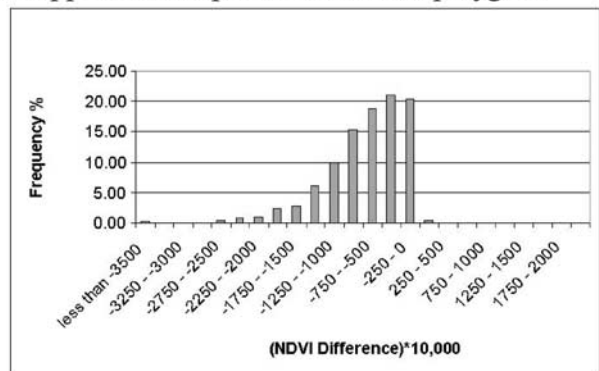


Figure 9. The histograms of NDVI*10,000 for the six scenarios shown in Figure 8.

HANDS. Unless they result from rapid green-up following fires, they are likely to be surface fires, lightly burned areas, or nonburned islands, especially for those with NDVI change close to zero or even positive.

[31] Figures 8b and 9b show all burned areas mapped by the HANDS both inside and outside the fire polygons. Since all pixels (6366) passed the threshold, their NDVI values

decrease by at least 0.039. Note that the number of pixels outside fire polygons amounts to 1891.

[32] Figures 8c and 9c show pixels inside the fire polygons that were not mapped by HANDS. 60% of these (766) did not pass the NDVI threshold, while 40% (506) passed the NDVI threshold but the number of CBP was less than 10% for each cluster. The former may represent nonburned

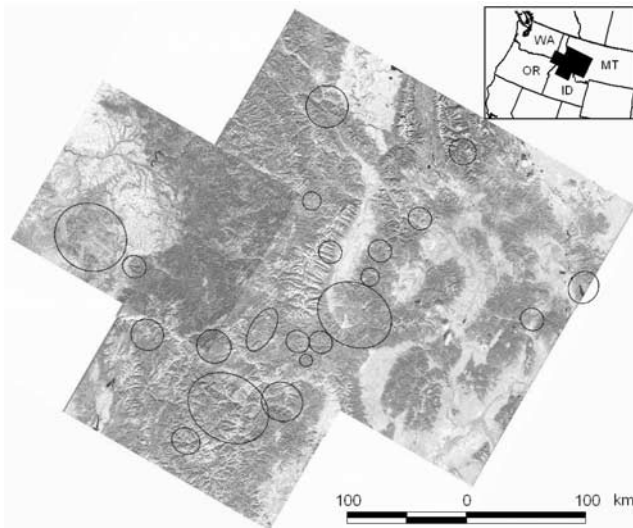


Figure 10. Mosaic of Landsat-7 TM quick-look images acquired between Sept 13 and Oct 8, 2000 with visible burned areas circled. See color version of this figure at back of this issue.

patches of tree canopy inside the fire polygons, which is evident from a mosaic of high-resolution LANDSAT TM scenes acquired over the region (Figure 10). Dark shades inside the circles are fire scars that exhibit varying degree of burning and topographic effects, producing a pattern with high spatial variability. It is likely that no manual survey can provide the level of detailed fire mapping possible with LANDSAT TM. The 40% remaining pixels appear in clusters (not random) within the fire polygons. They are more likely to be true fires but disqualified for lacking active fires. Hot spot detection frequency is thus an important consideration for the mapping algorithm used here.

[33] Figures 8d and 9d show those pixels that were mapped neither by HANDS nor by the active fire detection algorithm. 38.4% of these (437 pixels) failed to pass the HANDS threshold and the remaining (61.6% or 701 pixels) passed the threshold but contained no or insufficient number of CBP. For Figures 8c, 8d, 9c, and 9d, the majority of pixels show little change or increase in NDVI, suggesting nonburning of tree crowns. Those of large magnitude of negative NDVI correspond to no or too few active fires, attesting to real fires.

[34] Figures 8e and 9e show pixels (754) detected as hot spots but not mapped by HANDS. These pixels all have positive NDVI changes, and are unlikely to be real fires, although they could be very small fires at a scale ± 1 km, which AVHRR can detect. This suggests that the HANDS may be used to eliminate false hot spots except for such ecosystem that recovers quickly after burning such as tropical grassland or shrub. Usually, the signal of burned scars remains for a long period of time after fire.

[35] Figures 8f and 9f show pixels that are outside the fire polygons but were identified as burned area by HANDS. A considerable portion of these is located adjacent to the fire polygons. Large and small clusters of burned pixels are also found elsewhere, especially in the northwest corner where fire survey seems not been conducted. These pixels are

accompanied by both active fires and significant NDVI decrease that are more likely to be real fires.

[36] Figure 11 shows the correlation of burned area between fire clusters mapped by HANDS and fire polygons. We chose 131 cases that have relatively clear fire boundaries to differentiate between different fire events. They cover the bulk of burned area. The linear correlation coefficient is 0.9875, slope 1.0563, and intercept -0.0805 . Note that the relationship has less scatter as burn size increases.

5. Concluding Remarks

[37] In an effort to develop an inventory of wild fires in North America, 1-km AVHRR data acquired by a series of NOAA polar orbiting satellite since 1985 are being processed. This paper evaluates the algorithms used for both detecting active fires [Li *et al.*, 2000a] and mapping burned area [Fraser *et al.*, 2000]. These algorithms were designed originally for application across the Canadian boreal forest ecosystem using AVHRR/NOAA 14 data. Extension of their applications to other regions in NA with different AVHRR sensors is subject to quantitative evaluation, as presented in this paper. The algorithm for detecting active fires was assessed by applying it to both NOAA 11 and NOAA 14 data acquired in the United States and Canada; and the algorithm for mapping burned area was applied to major fire episodes occurred in U.S. western states in 2000 where extensive ground-based fire polygon data were made available by the U.S. forest services. Note that the algorithms have been tested extensively across Canada.

[38] Despite noticeable radiometric and observational differences between AVHRR onboard NOAA 11 and NOAA 14, the algorithm of Li *et al.* [2000a] proved to be well suitable for application with AVHRR from both satellites. Since tests for these sensors span throughout their lifetime (1989–2000) during which both observation geometry and radiometric characteristics drifted considerably, the tests bode well for their applications to other AVHRR sensors. However, when the algorithms were applied to

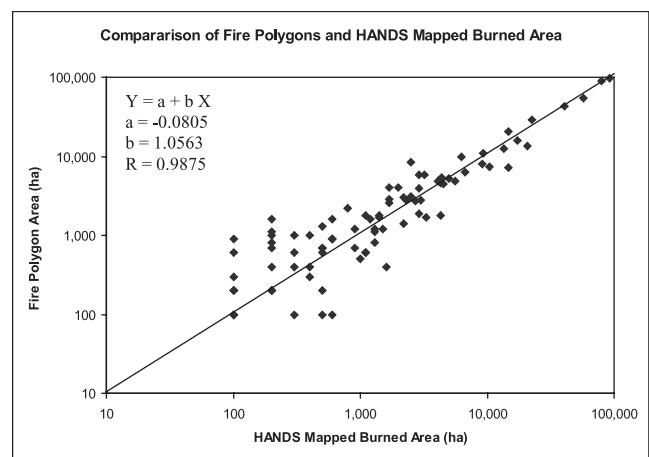


Figure 11. Comparison of burned area size from individual fires based on ground-based observation and satellite mapping. Statistical variables of a linear regression are given.

different ecosystems encountered in the United States, some problems emerged. A large number of commission and omission errors occurred over semi-arid regions covered by thin clouds. False fires caused by sun-glint occurred adjacent to rivers and around the edge of lakes where inaccurate registration failed to identify them. The problem is ameliorated by modifying the threshold in one of the tests included in the detection algorithm, and adding one more test for excluding sun-glint effect. The problem persists over dry and hot arid regions for which there appears to be inherent difficulties posed to any AVHRR-based fire detection [Csizsar *et al.*, 2002]. On the other hand, the algorithm perform very well over forest-covered regions where large and durable fires usually take place that account for the bulk of emissions in greenhouse gases and aerosol particulates.

[39] Given the above findings and availability of ground-based fire polygon data, the HANDS mapping method was evaluated using the forest fires that occurred in five Rocky states, primarily in Idaho and Montana. Overall, HANDS mapped 76% of burned area within the fire polygons. 13% of the area insider the polygons showed no sign of burning in terms of both active fire and change in vegetation greenness, which are likely to be nonburned islands or light surface burning. Eight percent of the polygon area not mapped by HANDS showed significant decreases in vegetation index but with no hot spots or fewer than that required to confirm a burned area. Hot spots could be missed due to cloud cover and infrequent satellite observation. Two percent of the area that was missed by the HANDS was located on the perimeter of the polygons that showed less degree of burning. A significant area of burn scars was mapped outside of the polygons that appear to be related to fires. In addition to the areal estimates, the location and shapes of burned scars are matched fairly well between ground-based and satellite techniques.

[40] Further analyses indicate that failure to map certain burned areas may result from the following factors:

1. It may result from the lack of hot spots detected. HANDS requires that 10% of a potential burn patch contains hot spots, which was intended to eliminate false burned area due to nonburning events, but may also eliminate real burns as well. The criterion needs to be optimized so that it does not lower the omission errors at the expense of increasing commission errors. The criterion may vary with land cover type.

2. Burned areas were rapidly greening up, which attenuates the NDVI changes during the period of determining NDVI difference. This is likely for fires occurring in early season. To remedy the problem, it is recommended that some burned area be mapped based on hot spot only, such as in the case of a cluster of hot spots.

3. It may result from partially burned pixels. Pixels on the edges of burned area or even inside major fires may be burned to a varying extent. Depending on the definition of burning, they may or may not be mapped as burned or nonburned pixels.

[41] In light of the various uncertainties, we conclude that the fire detection and mapping algorithms with a few minor adjustments are generally adequate for developing a fire inventory using multi-AVHRR data with creditable results over the forest ecosystem in NA. However, in application to nonforested areas, the detection results will be less reliable.

[42] **Acknowledgments.** The study was supported by NASA grant NAG510898 under its Land Cover and Land Use Change (LCLUC) program. Partial assistance was provided by the National Science Foundation of China (NSFC40028503). We thank Simon Pinnock from the Joint Research Centre of the European Commission for advice in developing the sun-glint screening test.

References

- Arino, O., *et al.*, Mapping of burned surfaces in vegetation fires, in *Global and Regional Vegetation Fire Monitoring From Space: Planning and Coordinated International Effort*, edited by F. Ahern, J. G. Goldammer, and C. Justice, pp. 227–255, SPB Acad., The Hague, 2001.
- Chen, J. M., W. J. Chen, J. Liu, J. Cihlar, and S. Gray, Annual carbon balance of Canada's forest during 1895–1996, *Global Biogeochem. Cycles*, *14*, 839–850, 2000.
- Cihlar, J., *et al.*, GeoComp-N, An advanced system for the processing of coarse and medium resolution satellite data, part 2, Biophysical products for northern ecosystems, *Can. J. Remote Sens.*, *28*, 21–44, 2002.
- Crutzen, P. J., L. E. Heidt, J. P. Krasnec, W. H. Pollock, and W. Seiler, Biomass burning as a source of atmospheric gases, CO, H₂O, N₂O, NO, CH₃CL and COS, *Nature*, *282*, 253–256, 1979.
- Csizsar, I., A. Abuelgasim, J. Jin, and Z. Li, Interannual changes of active fire detectability from long-term records of the advanced very high resolution radiometer, *107*, doi:10.1029/2001JD001373, in press, 2002.
- Dozier, J., A method for satellite identification of surface temperature fields of subpixel resolution, *Remote Sens. Environ.*, *11*, 221–229, 1981.
- Dwyer, E., J.-M. Gregoire, and J.-P. Malingreau, A global analysis of vegetation fires using satellite images: Spatial and temporal dynamics, *Ambio*, *27*, 175–181, 1998.
- Elvidge, C. D., K. E. Baugh, V. R. Hobson, E. A. Kihn, and H. W. Kroehl, Detection of fires and power outages using DMSP-OLS data, in *Remote Sensing Change Detection: Environmental Monitoring Methods and Applications*, edited by R. S. Lunetta and C. D. Elvidge, pp. 123–135, Ann Arbor Press, Chelsea, Mich., 1999.
- Fan, S., M. Gloor, J. Mahlman, S. Pacala, J. Sarmiento, T. Takahashi, and P. Tans, A large terrestrial carbon sink in North America implied by atmospheric and oceanic carbon dioxide data and models, *Science*, *282*, 442–446, 1998.
- Fernandez, A., P. Illera, and J. L. Casanova, Automatic mapping of surfaces affected by forest fires in Spain using AVHRR NDVI composite image data, *Remote Sens. Environ.*, *60*, 153–162, 1997.
- Flannigan, M. D., and T. H. Vonder Haar, Forest fire monitoring using NOAA satellite AVHRR, *Can. J. For. Res.*, *16*, 975–982, 1986.
- Flasse, S. P., and P. Ceccato, A contextual algorithm for AVHRR fire detection, *Int. J. Remote Sens.*, *17*, 419–424, 1996.
- Fraser, H. R., Z. Li, and J. Cihlar, Hotspot and NDVI differencing synergy (HANDS): A new technique for burned area mapping over Boreal Forest, *Remote Sens. Environ.*, *74*, 362–376, 2000.
- Fung, I., The global carbon cycle and atmospheric record: "The problem definition," in *Forest Ecosystems, Forest Management and the Global Carbon Cycle*, edited by M. J. Apps and D. T. Price, *NATO ASI Ser., Ser. I*, *40*, 25–34, 1996.
- Grégoire, J.-M., D. R. Cahoon, D. Stroppiana, Z. Li, S. Pinnock, H. Eva, O. Arino, J. M. Rosaz, and I. Csizsar, Forest fire monitoring and mapping for GOF: Current products and information networks based on NOAA-AVHRR, ERS ATSR, and SPOT-VGT, in *Global and Regional Vegetation Fire Monitoring From Space: Planning and Coordinated International Effort*, edited by F. Ahern, J. G. Goldammer, and C. Justice, pp. 105–124, SPB Acad., The Hague, Netherlands, 2001.
- Gutman, G., C. D. Elvidge, I. Csizsar, and P. Romanov, NOAA archive of data from meteorological satellite useful for fire product, in *Global and Regional Vegetation Fire Monitoring From Space: Planning and Coordinated International Effort*, edited by F. Ahern, J. G. Goldammer, and C. Justice, pp. 257–265, SPB Acad., The Hague, Netherlands, 2001.
- Hansen, J., R. Ruedy, M. Sato, and R. Reynolds, Global surface temperature in 1995: Return to pre-Pinatubo level, *Geophys. Res. Lett.*, *23*, 1665–1668, 1996.
- Hao, W. M., D. E. Ward, G. Olbu, and S. P. Baker, Emissions of CO₂, CO, and hydrocarbons from fires in diverse African savanna ecosystems, *J. Geophys. Res.*, *101*, 23,577–23,584, 1996.
- Harris, A. J., Towards automated fire monitoring from space: Semi-automated mapping of the January 1994 New South Wales wildfires using AVHRR data, *Int. J. Wildland Fire*, *6*, 107–116, 1996.
- Ichoku, C., Y. Kaufman, L. Giglio, Z. Li, R. H. Fraser, J. Jin, and B. Park, Comparative analysis of daytime fire detection algorithms using AVHRR data for the 1995 fire season in Canada: Perspective for MODIS, *Int. J. Remote Sens.*, in press, 2002.

- International Panel on Climate Change (IPCC), *Climate Change: The IPCC Scientific Assessment*, edited by J. T. Houghton et al., Cambridge Univ. Press, New York, 1990.
- International Panel on Climate Change (IPCC), *Climate Change: The IPCC Scientific Assessment*, 198 pp., Cambridge Univ. Press, New York, 1995.
- Justice, C. O., J. D. Kendall, P. R. Dowty, and R. J. Scholes, Satellite remote sensing of fires during the SAFARI campaign using NOAA advanced very high resolution radiometer data, *J. Geophys. Res.*, *101*, 23,851–23,863, 1996.
- Kasischke, E. S., and N. H. French, Locating and estimating the areal extent of wildfires in Alaskan boreal forests using multiple-season AVHRR NDVI composite data, *Remote Sens. Environ.*, *51*, 263–275, 1995.
- Kaufman, Y. J., C. J. Tucker, and I. Fung, Remote sensing of biomass burning in the tropics, *J. Geophys. Res.*, *95*, 9927–9939, 1990.
- Kaufman, Y. J., C. Justice, L. Flynn, J. Kendall, E. Prins, D. E. Ward, P. Menzel, and A. Setzer, Potential global fire monitoring from EOS-MODIS, *J. Geophys. Res.*, *103*, 32,215–32,238, 1998.
- Kennedy, P. J., A. S. Belward, and J.-M. Gregoire, An improved approach to fire monitoring in West Africa using AVHRR data, *Int. J. Remote Sens.*, *15*, 2235–2255, 1994.
- Levine, J. S., W. R. Cofer III, D. R. Cahoon, and E. L. Winstead, Biomass burning: A driver for global change, *Environ. Sci. Technol.*, *29*, 120–125, 1995.
- Li, Z., J. Cihlar, L. Moreau, F. Huang, and B. Lee, Monitoring fire activities in the boreal ecosystem, *J. Geophys. Res.*, *102*, 29,611–29,624, 1997.
- Li, Z., S. Nadon, and J. Cihlar, Satellite detection of Canadian boreal forest fires: Development and application of an algorithm, *Int. J. Remote Sens.*, *21*, 3057–3069, 2000a.
- Li, Z., S. Nadon, J. Cihlar, and B. J. Stocks, Satellite mapping of Canadian boreal forest fires: Evaluation and comparison and comparisons, *Int. J. Remote Sens.*, *21*, 3071–3082, 2000b.
- Li, Z., Y. J. Kaufman, C. Ithoku, R. Fraser, A. Trishchenko, L. Giglio, J. Jin, and X. Yu, A review of AVHRR-based active fire detection algorithms: Principles, limitations, and recommendations, in *Global and Regional Vegetation Fire Monitoring From Space: Planning and Coordinated International Effort*, edited by F. Ahern, J. G. Goldammer, and C. Justice, pp. 199–225, SPB Acad., The Hague, 2001.
- Martin, M. P., and E. Chuvieco, Mapping and evaluation of burned land from multi-temporal analysis of AVHRR NDVI images, *EARSel Adv. Remote Sens.*, *4*, 7–13, 1995.
- Pereira, J. M. C., A comparative evaluation of NOAA/AVHRR vegetation indices for burned surface detection and mapping, *IEEE Trans. Geosci. Remote Sens.*, *37*, 217–226, 1999.
- Pereira, A. C., and A. W. Setzer, Comparison of fire detection in savannas using AVHRR's channel 3 and TM images, *Int. J. Remote Sens.*, *17*, 1925–1937, 1996.
- Prins, E. M., and W. P. Menzel, Geostationary satellite detection of biomass burning in South America, *Int. J. Remote Sens.*, *13*, 2783–2799, 1990.
- Ramsey, M. S., and J. R. Arrowsmith, New images of fire scars may help mitigate future natural hazards, *Eos Trans. AGU*, *82*(36), 393, 397–398, 2001.
- Randriambelo, T., S. Baldy, M. Bessafi, M. Petit, and M. Despinoy, An improved detection and characterization of active fires and smoke plumes in south-eastern Africa and Madagascar, *Int. J. Remote Sens.*, *19*, 2623–2638, 1998.
- Rao, C. R. N., and J. Chen, Post-launch calibration of the visible and near-infrared channels of the advanced very high resolution radiometer on NOAA-14 spacecraft, *Int. J. Remote Sens.*, *17*, 2743–2747, 1996.
- Roy, D. P., L. Giglio, J. D. Kendall, and C. O. Justice, Multi-temporal active-fire based burn scar detection algorithm, *Int. J. Remote Sens.*, *20*, 1031–1038, 1999.
- Setzer, A. W., and M. C. Pereira, Amazonia biomass burnings in 1987 and an estimate of their tropospheric emissions, *Ambio*, *20*, 19–22, 1991.
- Setzer, A. W., and M. C. Pereira, Operational detection of fires in Brazil with NOAA-AVHRR, paper presented at 24th International Symposium on Remote Sensing of the Environment, Environ. Res. Inst. of Mich., Rio de Janeiro, 1992.
- Tans, P. P., I. Y. Fung, and T. Takahishi, Observational constraints on the global CO₂ budget, *Science*, *247*, 1431–1438, 1990.
- Townshend, J. R. G., Global data sets for land applications from the advanced very high resolution radiometer: An introduction, *Int. J. Remote Sens.*, *15*, 3319–3332, 1994.
- Weber, G., and B. Stocks, Forest fires and sustainability in the boreal forest of Canada, *Ambio*, *27*, 545–550, 1998.
- Williams, E. R., The Schumann resonance: A global tropical thermometer, *Science*, *256*, 1184–1187, 1992.
-
- A. A. Abuelgasim and R. Fraser, Canada Centre for Remote Sensing, 588 Booth Street, Ottawa, Ontario, Canada K1A 0Y7.
- I. Csiszar, Office of Research and Applications, NOAA/NESDIS, 5200 Auth Road, Camp Springs, MD 20746-4304, USA.
- P. Gong and R. Pu, Department of Environmental Sciences, 260 Mulford Hall, University of California, Berkeley, CA 94720-3100, USA.
- W. Hao, Fire Sciences Laboratory, RMRS, USDA Forest Service, Missoula, MT 59807, USA.
- J. Jin and Z. Li, Department of Meteorology, 224 CSS Building, Room 2207, University of Maryland, College Park, MD 20742-2465, USA. (zli@atmos.umd.edu)

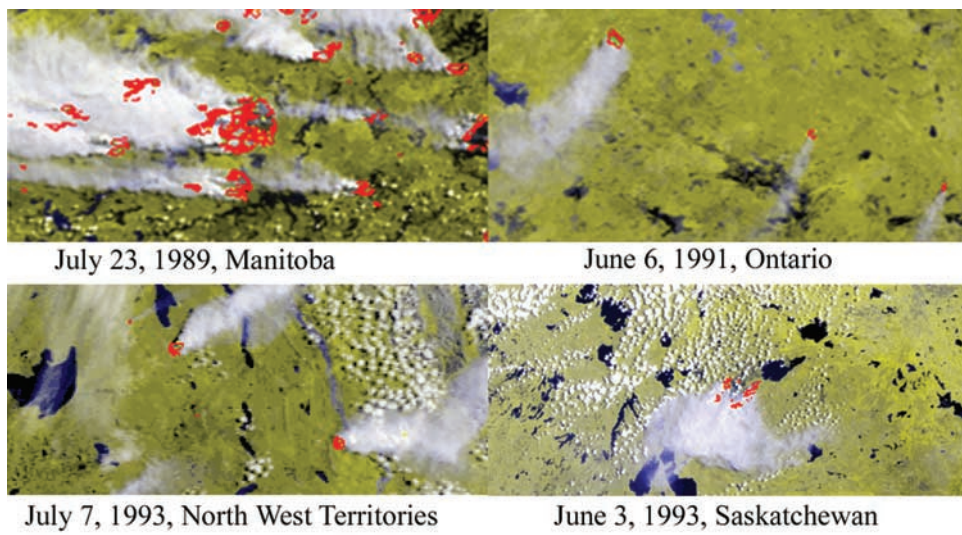


Figure 1. Fire locations identified using the algorithm of *Li et al.* [2000a] applied to different regions of Canada and different years spanning the lifetime of NOAA 11. Hots pots (red pixels) are superimposed over an AVHRR false color composite (RGB = 2, 2, 1).

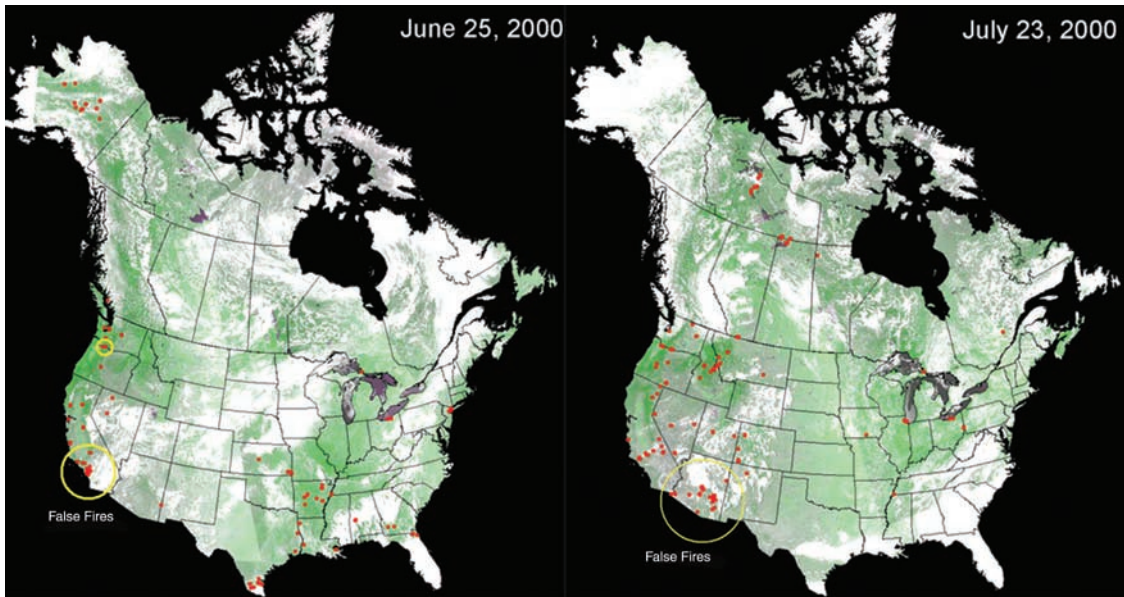


Figure 2. Active fire detection results across the United States and Canada for two sample dates during the summer of 2000 (hot spots are shown as enlarged red points, clouds appear white, vegetation is green, and yellow circles identify questionable results).

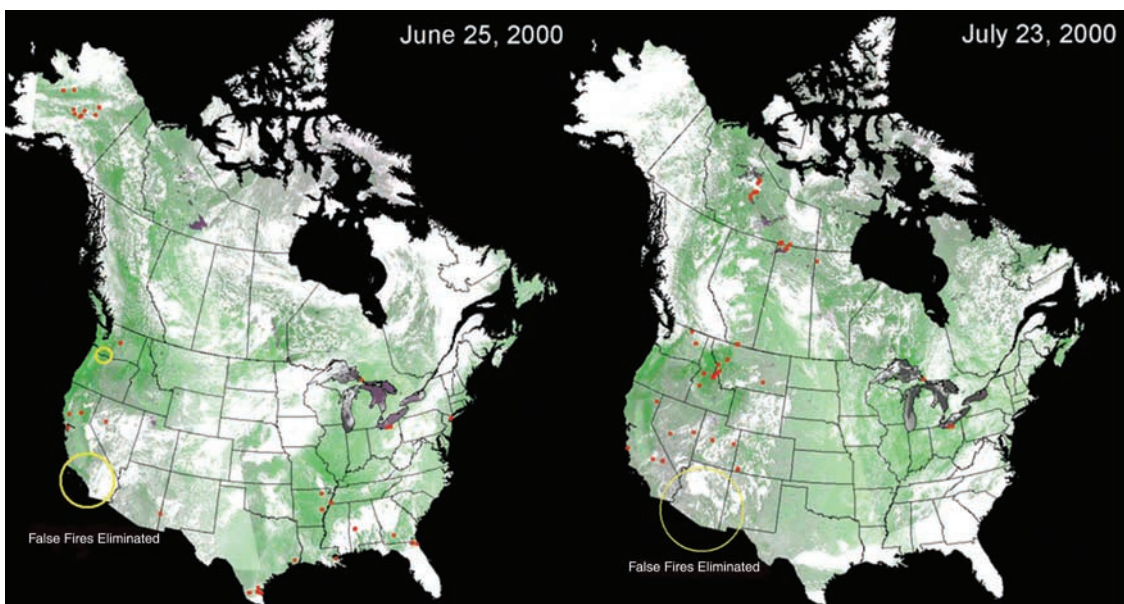


Figure 3. Same as in Figure 3, but based on the modified algorithm.

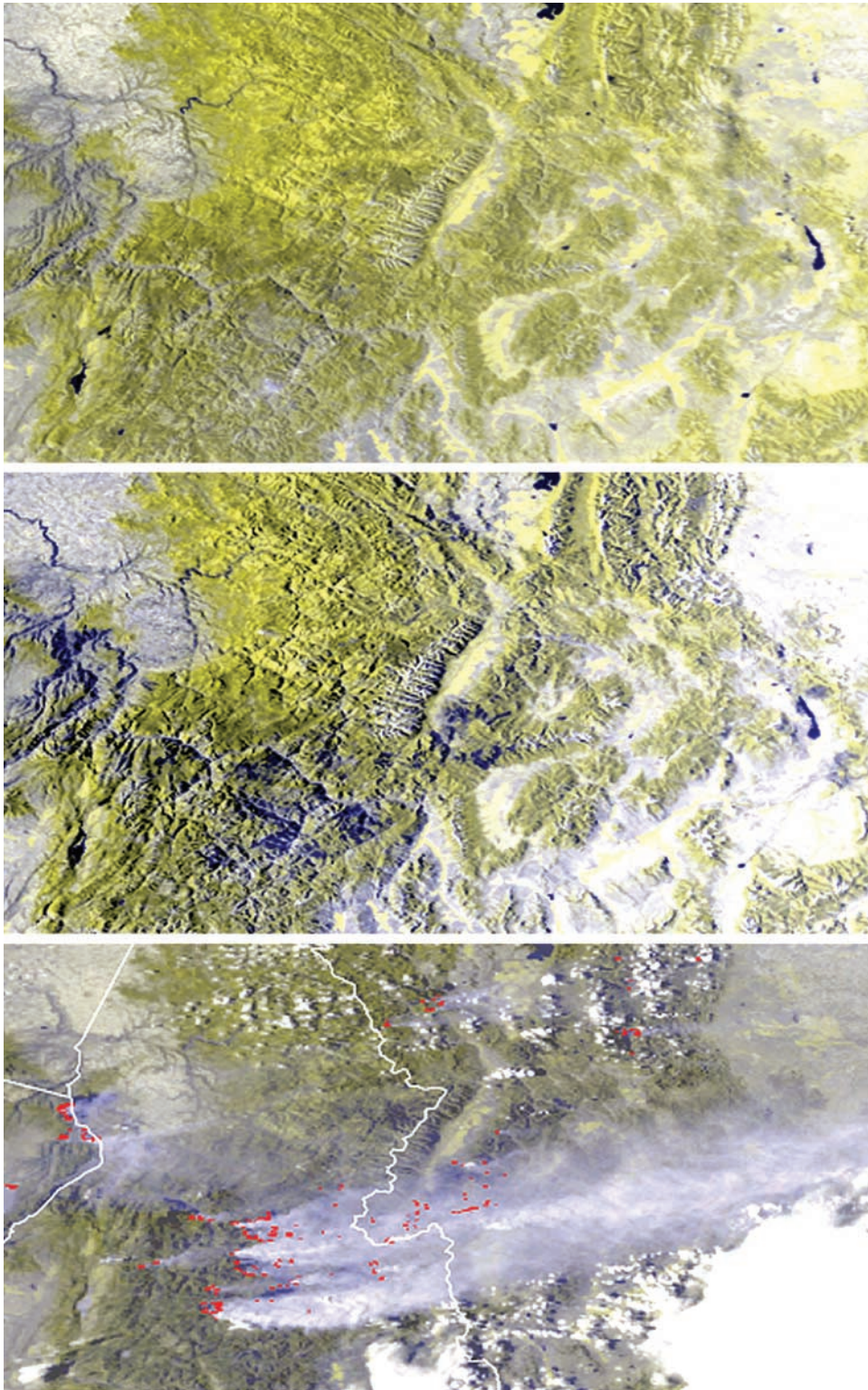


Figure 4. AVHRR clear-sky composites before (top) and after (middle) fires occurring in 2000. Bottom image shows fire hot spots detected on Aug. 26, 2000.

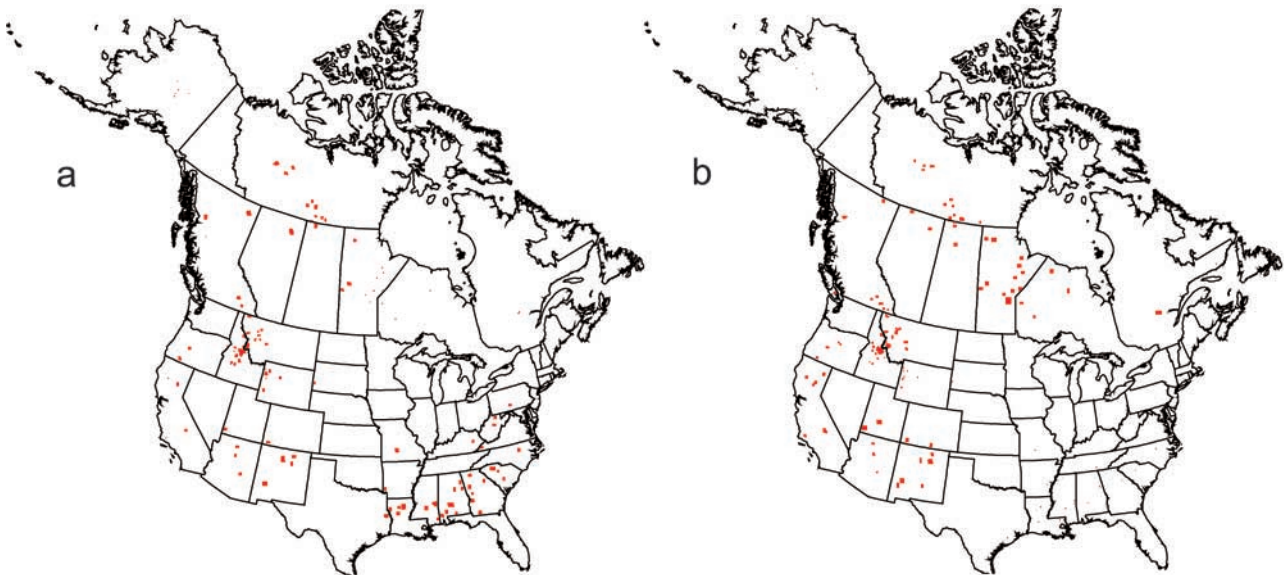


Figure 5. The distributions of fire hot spots (a: left) and total burned area (b: right) detected from AVHRR across North America in 2000.

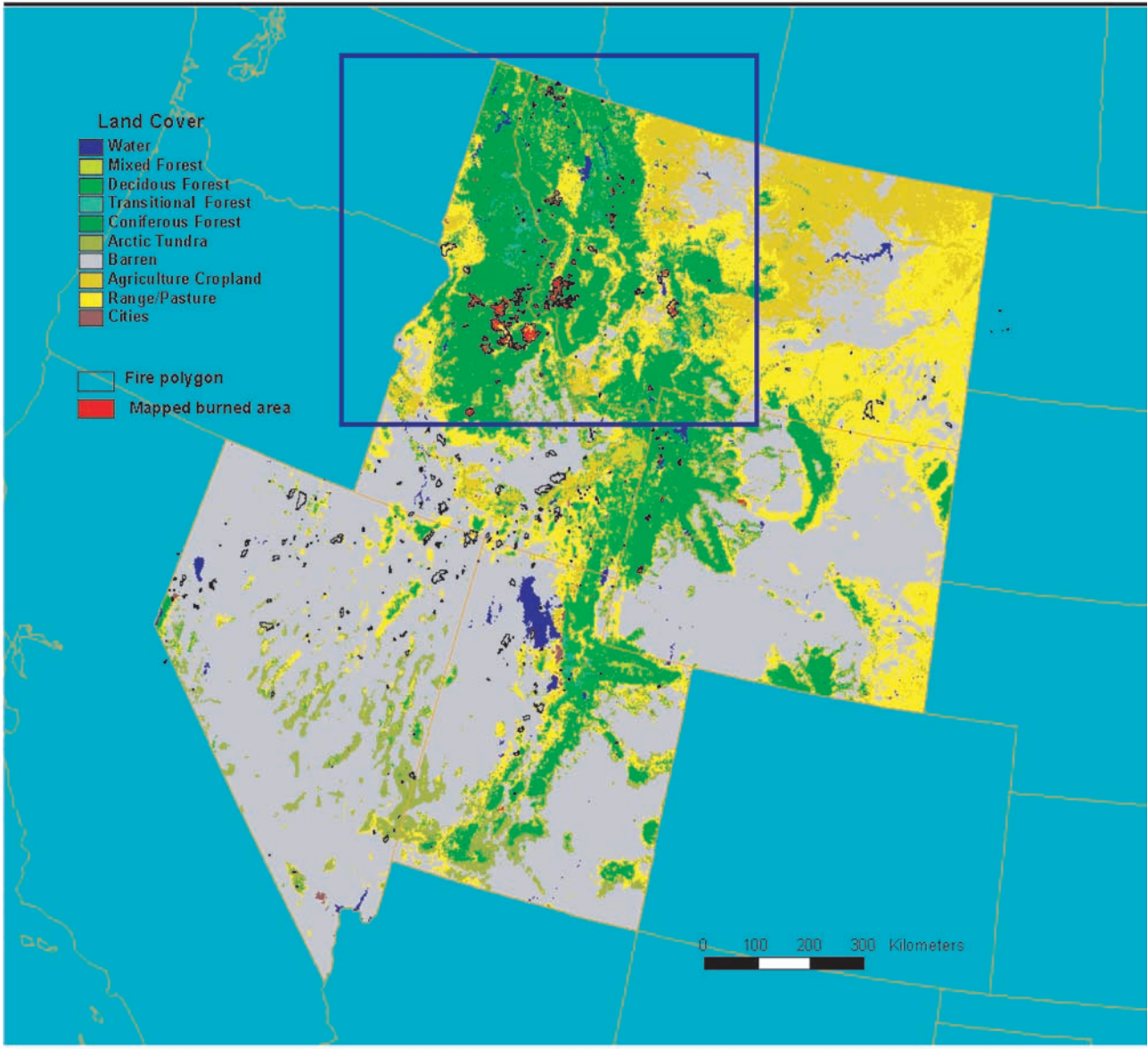


Figure 6. Comparison of satellite mapped burned area (red) and ground-based fire polygons in five western states. Background colors denote different land cover types.

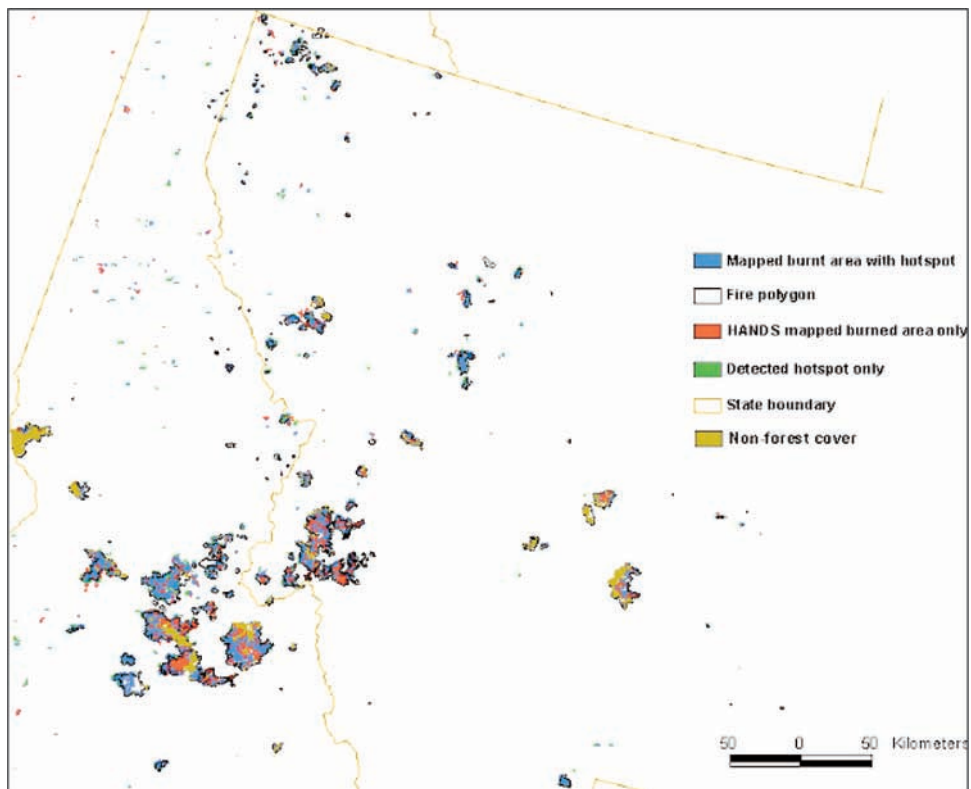
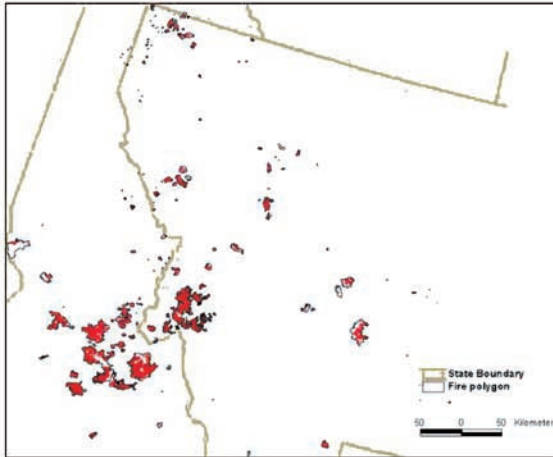
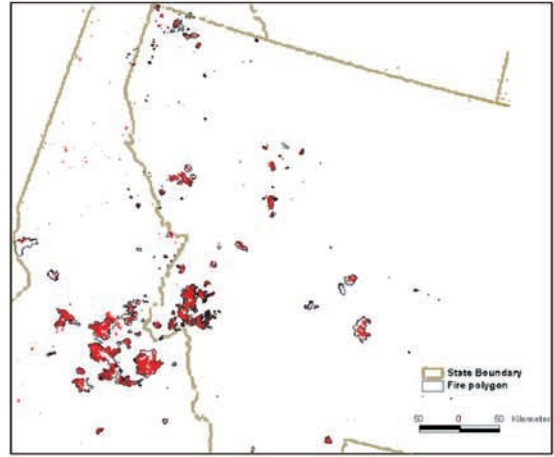


Figure 7. Fire mapping results classified by source and algorithm inside the selected area shown in Figure 7. Different colors differentiate between fire polygons, non-forest-covered regions, and state boundaries.

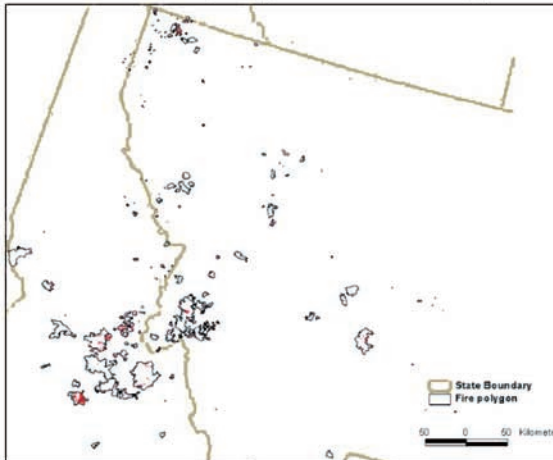
a all pixels inside the polygons



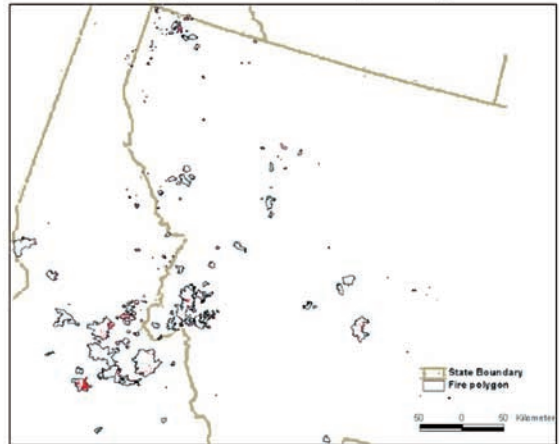
b all mapped fire pixels



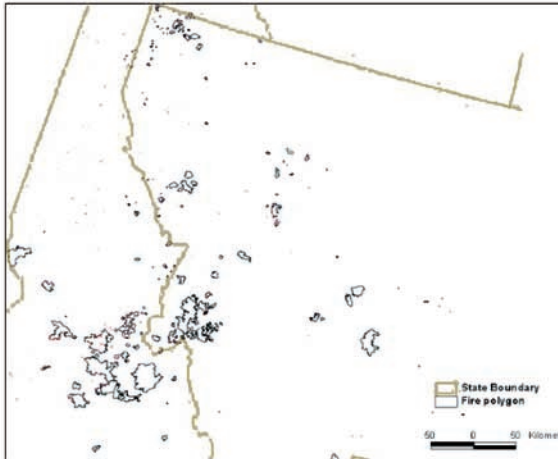
c pixels inside the polygons but not mapped



d fires not mapped for lacking hot spots



e hot spot pixels but not mapped



f mapped burned pixels outside the polygons

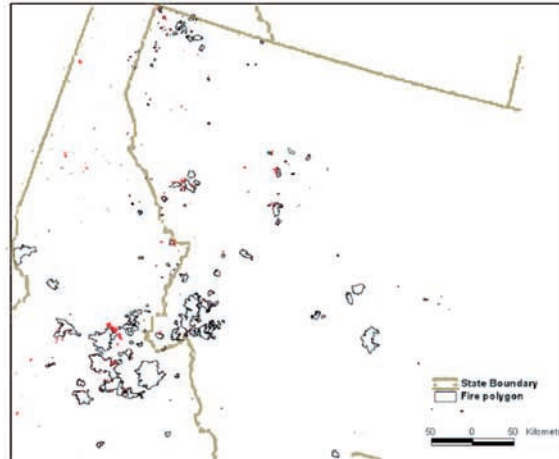


Figure 8. Analysis of fire detection results under different scenarios: (a) all pixels inside the fire polygons excluding nonforest regions, (b) all mapped fire pixels inside and outside the polygons, (c) pixels inside the polygons but not mapped, (d) inside the polygons not mapped due to lack of hot spots, (e) hot spot pixels but not mapped, and (f) mapped burned pixels outside the polygons.

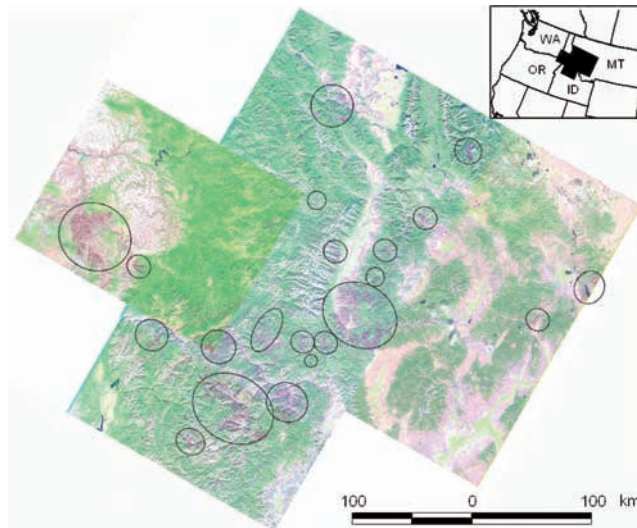


Figure 10. Mosaic of Landsat-7 TM quick-look images acquired between Sept 13 and Oct 8, 2000 with visible burned areas circled.